Microstructure and mechanical behavior of cross-linked biopolymer networks

Zagar, Goran

Chapter 3

The microstructure

Based on: G. Žagar, P.R. Onck and E. Van der Giessen, "*The microstructure of Isotropically Cross-linked Filamentous networks*", in preparation.

In-vitro cross-linked biopolymer networks are popular model systems for studying the mechanics of living cells (Bausch and Kroy, 2006; Lieleg et al., 2010). Besides depending on filaments and cross-linking molecules, the mechanical properties of these networks are highly dependent on their microstructure (Shin et al., 2004; Gardel et al., 2004a; Lieleg et al., 2007). However, detailed information about the microstructure is difficult to obtain experimentally, if only because individual filaments are often too thin to be observed. Until now, microstructural information could only be retrieved by inverse modelling using theoretical models (Tharmann et al., 2007; Lin et al., 2010b; Yao et al., 2010). In this chapter, a mere topological consideration is used to derive analytical expressions for the relationship between the microstructure of three-dimensional (3D) random networks of cross-linked filaments and measurable properties, such as the constituent concentrations and the average filament length l_0. Moreover, it will be shown that the key length scale of the microstructure, i.e. the mean distance between two neighbouring cross-links along the filament, l_c, scales with the $-1/3$rd power of the cross-link concentration. The generality of here presented approach promises applicability to a wide range of isotropically cross-linked filamentous networks.

3.1 The network topology

We start out by generating periodic 3D representative volume element (RVE) of isotropic and cross-linked random networks of individual semi-flexible filaments

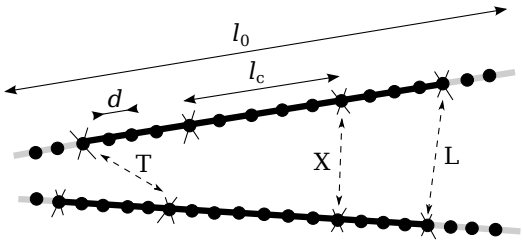

Figure 3.1. Two filaments of length l_0 making an L, T or X cross-link. The binding sites for cross-linking molecules (dots) are separated on average by the length d. The sites where filament are cross-linked (crosses) are separated on average by the length l_c. On average, each filament has two dangling ends (gray) of length l_c.

(see § 2.2 and § 2.3 for details) (Huisman et al., 2007).

The mechanical behavior of generated RVEs is controlled by the percolating *subnetwork* that excludes the filament dangling ends (the filament sections that are free on one end) as well as any isolated (i.e., disconnected) filament clusters, since these cannot deform under macroscopic load. By disregarding the dangling ends, the cross-link coordination of the subnetwork is either 4, 3 or 2, which we refer to as X-, T- or L-type cross-links, respectively (Figure 3.1). The subnetwork can be seen as a *connected graph* where L-, T- and X-cross-links are the *vertices* and the filament sections are the *edges* of the graph. The connected graph associated to the subnetwork is fully defined in terms of the number of sections n_s, the number of cross-links n_{cl} and the number of the three types of cross-links, i.e. n_L, n_T and n_X, respectively. These five topological parameters are related by two " conservation" equations:

$$1 = \tilde{n}_L + \tilde{n}_T + \tilde{n}_X, \tag{3.1a}$$

$$\tilde{n}_s = \frac{1}{2}\left(2\tilde{n}_L + 3\tilde{n}_T + 4\tilde{n}_X\right), \tag{3.1b}$$

where $\tilde{n}_s = n_s/n_{cl}$ and $\tilde{n}_L$, $\tilde{n}_T$ and $\tilde{n}_X$ are relative fractions of L-, T- and X-coordinated cross-links, respectively. The latter three are all defined between 0 and 1, while the ratio $\tilde{n}_s$ ranges from 1 (for $\tilde{n}_L = 1$) to 2 (for $\tilde{n}_X = 1$).

The fractions $\tilde{n}_L$, $\tilde{n}_T$ and $\tilde{n}_X$ represent the probabilities that a randomly chosen cross-link is either of L-, T- or X-type, and these have to be equal to the probabilities that two filaments form such cross-links. Since a filament of mean length l_0 comprising sections (two dangling ends included) with mean length l_c contains $(l_0 - l_c)/l_c$ cross-linking sites (Figure 3.1), the probability of choosing a random

cross-linking site in one filament is $1/(\tilde{l}_0 - 1)$, with $\tilde{l}_0 = l_0/l_c$. The probability of choosing an outer cross-linking site is $2/(\tilde{l}_0 - 1)$, while the probability of choosing an inner site is $(\tilde{l}_0 - 3)/(\tilde{l}_0 - 1)$. Because the merger of outer sites of two filaments gives rise to L cross-links, an inner and an outer site to T cross-links and two inner sites to X cross-links, the relative fractions $\tilde{n}_L$, $\tilde{n}_T$ and $\tilde{n}_X$ are found as:

$$\tilde{n}_L = \frac{4}{(\tilde{l}_0 - 1)^2}, \quad \tilde{n}_T = 4\frac{\tilde{l}_0 - 3}{(\tilde{l}_0 - 1)^2}, \quad \tilde{n}_X = \frac{(\tilde{l}_0 - 3)^2}{(\tilde{l}_0 - 1)^2}. \tag{3.2}$$

Combination of (3.2) and (3.1b) gives

$$\tilde{n}_s = 2\frac{\tilde{l}_0 - 2}{\tilde{l}_0 - 1}, \tag{3.3}$$

revealing that the topology of the subnetwork depends only on a single parameter: the ratio $\tilde{l}_0 = l_0/l_c$.

The topology predicted by Eqs. (3.2) and (3.3) matches very well with the data extracted from the generated networks, as shown in Figure 3.2. The lower topological limit, $\tilde{l}_0 \to 3$, is the L-only subnetwork ($\tilde{n}_L = 1$) formed by a single percolation of filament sections with one section and two dangling ends per filament, thereby maximizing l_c to $l_0/3$. The other topological limit is the X-only subnetwork ($\tilde{n}_X = 1$) which is reached for $\tilde{l}_0 \to \infty$. Note that, because l_0 and l_c are arc-length measures along the filament, these parameters, Eq. (3.2) and Eq. (3.3) apply to straight as well as to undulated filaments.

3.2 Network equation

We continue by developing a connection between the topology of the subnetwork and the measurable or known properties of the whole network, namely the constituent concentrations.

A common measure of the mean distance between filaments is the mesh size ξ. For a cubic RVE of size W^3, we define the mesh size ξ through the mean volume associated to each section,

$$n_s l_c \xi^2 = W^3. \tag{3.4}$$

The mesh size ξ is uniquely related to the filament concentration c_s (in mg/ml) as

$$c_s = \frac{\rho_f \frac{\pi}{4} t^2 n_s l_c}{W^3} = \frac{\pi}{4}\rho_f \left(\frac{t}{\xi}\right)^2, \tag{3.5}$$

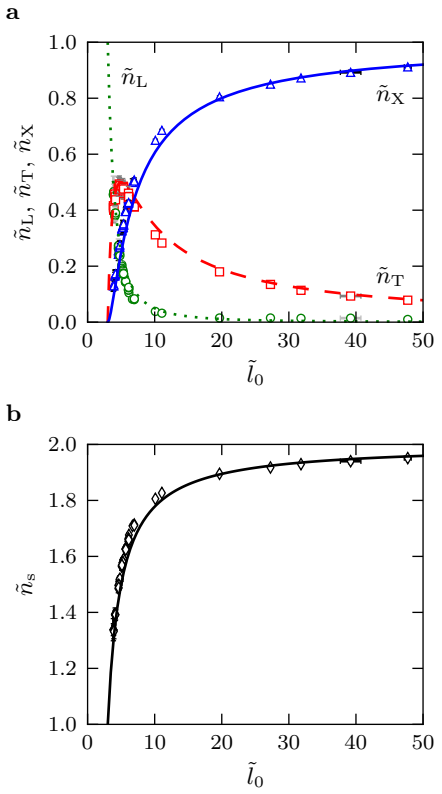

Figure 3.2. The topology of a random network. The parameters of the generated networks (symbols) as a function of $\tilde{l}_0$: **a**, $\tilde{n}_L$ (circle), $\tilde{n}_T$ (square) and $\tilde{n}_X$ (triangle) and **b**, $\tilde{n}_s$. The predictions according to (3.2) and (3.3) are shown with lines.

with ρ_f the density of the filament itself and t the filament diameter. When M_{cp} is the molecular mass of the cross-linking molecule, the concentration of cross-links in the subnetwork is

$$c_{cl} = n_{cl} \frac{M_{cp}}{W^3}. \tag{3.6}$$

The Eqs. (3.4)–(3.6) express the link between the morphology of the subnetwork and the concentration of its constituents. However, the parameters c_s and c_{cl} are not equal to the initial concentrations used to cross-link biopolymer networks *in vitro*, due to the presence of dangling ends and isolated clusters. Also, not all cross-linking molecules need to actually link two filaments (they may be dormant). Moreover, in experiments generally only the "total" constituent concentrations for

the sample are known. We will now show that these effects can be incorporated as well.

The total concentration of filaments, c_f, can be calculated in terms of the total number of filaments, n_f, in the RVE as

$$c_\mathrm{f} = \frac{\rho_\mathrm{f} \frac{\pi}{4} t^2 n_\mathrm{f} l_0}{W^3}. \tag{3.7}$$

From (3.5) and (3.7), the concentration ratio

$$\frac{c_\mathrm{s}}{c_\mathrm{f}} = \frac{n_\mathrm{sf}}{\tilde{l}_0} = 1 - \tilde{n}_\mathrm{L}, \tag{3.8}$$

is determined by the number of sections relative to the total number of filaments, $n_\mathrm{sf} = n_\mathrm{s}/n_\mathrm{f}$, but also by the probability $1 - \tilde{n}_\mathrm{L}$. The latter equality in (3.8) can be reasoned as follows. In percolation and graph theory (Albert and Barabasi, 2002), the infinite cluster in the supercritical phase ($p > p_\mathrm{c}$) grows as $S_\infty \propto p - p_\mathrm{c}$ near the percolation threshold, $p \to p_\mathrm{c}$, while the total size of the graph increases in proportion to the edge probability, $S \propto p$. In this context, the subnetwork with concentration c_s represents the infinite cluster for the RVE having total filament concentration c_f, so the ratio $c_\mathrm{s}/c_\mathrm{f} \equiv S_\infty/S \propto (p - p_\mathrm{c})/p$. Thus, in a network approaching the L-only limit, the filaments become mainly grouped into a larger number of smaller clusters that are disconnected from the subnetwork, thereby raising the difference between c_s and c_f. Because the percolation threshold for our RVE is the L-only network, we expect that $p_\mathrm{c}/p \equiv \tilde{n}_L$. This ansatz is confirmed in Figure 3.3 by the plot of $c_\mathrm{s}/c_\mathrm{f}$ versus $\tilde{l}_0$ as determined from the generated networks and by using Eq. (3.2) in Eq. (3.8).

From (3.8), c_s can now be solved as function of $\tilde{n}_L$ and assuming this topological parameter to be known, the mesh size ξ is obtained from (3.5) as

$$\xi^2 = \frac{\pi}{4} \frac{\rho_\mathrm{f} t^2}{c_\mathrm{f}} \frac{1}{1 - \tilde{n}_L}. \tag{3.9}$$

The mesh size given by (3.9) therefore, does not only have the dependence on concentration, $\xi \propto 1/\sqrt{c_\mathrm{f}}$ (Schmidt et al., 1989), but also depends on the network topology such that ξ is enhanced for lower connectivity.

In order to extend the consideration to the "total" concentration of cross-linking molecules in the RVE, defined as $c_\mathrm{cp} = n_\mathrm{cp} M_\mathrm{cp}/W^3$, we assume that all of the n_cp cross-linking molecules are bound to filaments, but that only a fraction of them are actually cross-linking two filaments. This assumption of having "decorated" filaments (as illustrated in Figure 3.1) is consistent with the observations by Shin

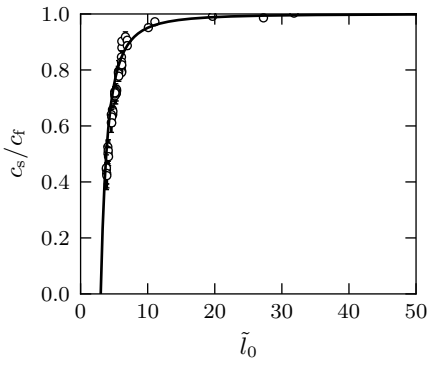

Figure 3.3. The subnetwork size. The c_s/c_f vs. $\tilde{l}_0$ for the generated networks (symbol) and the predictions according to the right-hand side in (3.8). The data sets are the same as in Figure 3.2.

et al. (2004) for *in-vitro* actin filament (F-actin) networks cross-linked by scruin. The concentration of the cross-linking molecules c_{cp} that decorates the filaments, can in principle, be measured using centrifugation assays; the c_{cp} then represents the concentration of the cross-linking molecules of the solid phase (pellet), which is the difference between the cross-linking molecule concentrations of the initial sample and the liquid phase (supernatant).

The definition of c_{cp} and Eq. (3.6) can be combined to give $c_{\mathrm{cp}}/c_{\mathrm{cl}} = n_{\mathrm{cp}}/n_{\mathrm{cl}}$, and the latter ratio can be expressed in terms of material and topological parameters as follows. The decoration of filaments with cross-linking molecules can be characterized by a mean distance d between two cross-linking molecule binding sites along a filament (Figure 3.1); obviously $d \leq l_{\mathrm{c}}$. The number of cross-linking molecules n_{cp}, therefore, can be estimated as the number of filaments n_{f} times the number of cross-linking molecule binding sites per filament, $l_0/d - 1$ (Figure 3.1). However, since this product counts each cross-link twice, it is diminished by n_{cl}, so that $n_{\mathrm{cp}} = n_{\mathrm{f}}(l_0/d - 1) - n_{\mathrm{cl}}$. By assuming a homogeneous concentration of cross-linking molecules in the RVE, we expect just one cross-linking molecule in the volume $d\,\xi^2$; therefore, $d \approx M_{\mathrm{cp}}/(c_{\mathrm{cp}}\,\xi^2)$ or with (3.4) and (3.6), $d \approx \tilde{n}_{\mathrm{s}} l_{\mathrm{c}}(c_{\mathrm{cl}}/c_{\mathrm{cp}}) = (n_{\mathrm{s}}/n_{\mathrm{cp}})l_{\mathrm{c}}$. Note that in this way, the estimated d becomes exact at high connectivity; the subnetwork then is the total network and the dangling ends vanish. From the above expression for n_{cp} and d with the use of the definition

for n_{sf}, after some manipulations we can write the ratio $c_{\mathrm{cp}}/c_{\mathrm{cl}} = n_{\mathrm{cp}}/n_{\mathrm{cl}}$ as

$$\frac{c_{\mathrm{cp}}}{c_{\mathrm{cl}}} = \frac{\tilde{n}_{\mathrm{s}} + n_{\mathrm{sf}}}{\tilde{l}_0 - n_{\mathrm{sf}}}. \tag{3.10}$$

Alternatively, $c_{\mathrm{cp}}/c_{\mathrm{cl}}$ can be obtained as the ratio of expressions (3.7) and (3.6), multiplied by the ratio $c_{\mathrm{cp}}/c_{\mathrm{f}}$ of measurable concentrations. Combining this with (3.10) and by expressing all topological parameter in terms of $\tilde{l}_0$ through (3.2), (3.3) and (3.8), we finally obtain:

$$\frac{(\tilde{l}_0 - 3)(\tilde{l}_0 + 1)(\tilde{l}_0^3 - 9\tilde{l}_0 + 4)}{2(\tilde{l}_0 - 2)(\tilde{l}_0 - 1)} = \frac{\pi t^2 \rho_{\mathrm{f}} l_0}{M_{\mathrm{cp}}} \frac{c_{\mathrm{cp}}}{c_{\mathrm{f}}}\,. \tag{3.11}$$

The right-hand side of (3.11) is defined in terms of measurable macroscopic concentrations or known material parameters for the constituents. The left-hand side is a function of a topological parameter $\tilde{l}_0 = l_0/l_{\mathrm{c}}$, where the only unknown is the length l_{c}. It is not possible to invert (3.11) in order to obtain an analytical expression for l_{c}, but the solution can readily be obtained numerically. Moreover, the asymptotic behavior for large $\tilde{l}_0$ can be easily extracted from the left-hand side of (3.11). Thus, by keeping only the highest powers of $\tilde{l}_0$, the behavior of the left-hand side in (3.11) for $\tilde{l}_0 \gg 3$ quickly converges towards $\tilde{l}_0^3/2$, leading to

$$l_{\mathrm{c}} = \left[\frac{M_{\mathrm{cp}}}{2\pi\rho_{\mathrm{f}}} \left(\frac{l_0}{t} \right)^2 \frac{c_{\mathrm{f}}}{c_{\mathrm{cp}}} \right]^{1/3}. \tag{3.12}$$

For constant c_{f} and constant l_0 then, (3.11) predicts the scaling

$$l_{\mathrm{c}} \propto {c_{\mathrm{cp}}}^{y} \tag{3.13}$$

with $y = -1/3$. Because the parameters l_0 and l_{c} are independent of the shape of the filament contour, as argued above, expressions (3.4) through (3.7) also inherit this independence, since they are all defined as a product of either a constant, a dimensionless topological number and/or the lengths l_0 or l_{c}. Therefore, (3.11) is expected to hold, at least, for isotropically cross-linked networks of semiflexible filaments.

In Figure 3.4, we show that the power $-1/3$ dependence of l_{c} on the concentration of cross-linking molecules c_{cp} obtained from (3.11) is consistent with available experimental data for isotropically cross-linked networks of semiflexible filaments; Tharmann et al. (2007) proposed a scaling exponent $y = -0.4$ for F-actin networks cross-linked by rigor heavy-meromyosin (HMM) proteins and an

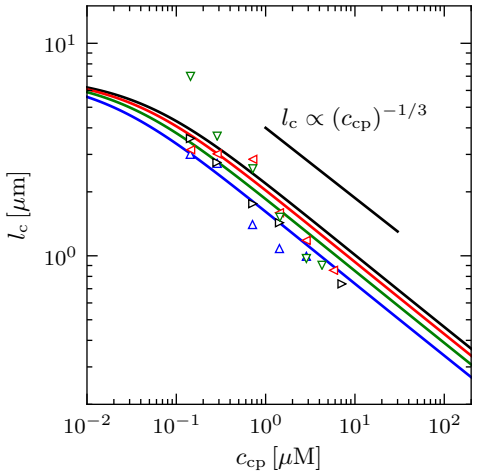

Figure 3.4. The microstructure of the F-actin/rigor-HMM networks. The mean distance between the cross-links along the filament l_c as a function of concentration of cross-linking molecule c_{cp}. Symbols show the data presented in Tharmann et al. (2007) for $l_0 = 21\,\mu$m and for c_f: $\triangle$ $9.5\,\mu$M, $\triangledown$ $14.3\,\mu$M, $\triangleleft$ $19\,\mu$M and $\triangleright$ $23.8\,\mu$M. The lines show the predictions according to (3.11) for same concentrations c_f and with additional parameters $\rho_f = 1300$ mg/mL, $t = 7$ nm (Schmidt et al., 1989), $M_{cp} = 405$ kDa (Young et al., 1965).

exponent $y = -0.2$ was recently suggested for ionically cross-linked networks of intermediate filaments (Lin et al., 2010b; Yao et al., 2010). However, whereas this experimental data (Tharmann et al., 2007; Lin et al., 2010b; Yao et al., 2010) are obtained indirectly by interpretation of the measured mechanical response through a theoretical model for network stiffness, Eqs. (3.11) and (3.12) are derived *solely* through topological considerations.

3.3 Conclusions

As demonstrated here, simple relationships between geometrical and topological parameters of isotropically cross-linked network can describe the microstructure to a great detail in terms of few measurable macroscopic parameters: the constituent concentrations and the average filament length. If extended to include effects like excluded volume, isotropic-to-nematic transition or filament bundling, it might be possible to apply the same approach to an even wider range of network-like materials.